Journal of Environmental Management 370 (2024) 122558

Contents lists available at ScienceDirect

Journal of Environmental Management

journal homepage: www.elsevier.com/locate/jenvman

Research article

Scalable mesoporous biochars from bagasse waste for Cu (II) removal: Process optimisation, kinetics and techno-economic analysis

Julius G. Bongosia [a], Amthal Al-Gailani [a], Ben W. Kolosz [b], Adrian Loy Chun Minh [c], Serene Sow Mun Lock [d], Kin Wai Cheah [e], Martin J. Taylor [a,*]

[a] School of Engineering, Chemical Engineering, University of Hull, Hull, HU6 7RX, United Kingdom
[b] Energy and Environment Institute, University of Hull, HU6 7RX, United Kingdom
[c] Department of Chemical Engineering, The University of Melbourne, Victoria, 3010, Australia
[d] Centre of Carbon Capture, Utilisation and Storage (CCCUS), Department of Chemical Engineering, Universiti Teknologi PETRONAS, 32610, Seri Iskandar, Malaysia
[e] School of Computing, Engineering & Digital Technologies, Teesside University, Middlesbrough, TS1 3BA, United Kingdom

ARTICLE INFO

Keywords:
Sugarcane bagasse Biochar
Mesoporous adsorbents
Cu (II) removal
Parametric modelling and optimisation
Lignocellulosic biomass waste
Environmental remediation

ABSTRACT

As the world faces the brink of climatological disaster, it is crucial to utilize all available resources to facilitate environmental remediation, especially by accommodating waste streams. Lignocellulosic waste residues can be transformed into mesoporous biochar structures with substantial pore capacity. While biochars are considered a method of carbon dioxide removal (CDR), they are in fact an environmental double-edged sword that can be used to extract metal ions from water bodies. Biochars possess high chemical affinities through chemisorption pathways that are tuneable to specific pH conditions. This work demonstrates how biochars can be enhanced to maximise their surface area and porosity for the removal of Cu (II) in solution. It was found that bagasse derived mesoporous biochars operate preferentially at high pH (basic conditions), with the 1.18 mKOH/mSCB material reaching 97.85% Cu (II) removal in 5 min. This result is in stark contrast with the majority of biochar adsorbents that are only effective at low pH (acidic conditions). As a result, the biochars produced in this work can be directly applied to ancestral landfill sites and carbonate-rich mine waters which are highly basic by nature, preventing further metal infiltration and reverse sullied water supplies. Furthermore, to assess the value in the use of biochars produced and applied in this way, a techno-economic assessment was carried out to determine the true cost of biochar synthesis, with possible routes for revenue post-Cu being removed from the biochar.

1. Introduction

Biochar has drawn significant practical attention and market value in recent years due to developing applications in; carbon capture and storage (Guo et al., 2022), soil fertility enhancement/flood management tools (Laird et al., 2010), catalyst support (Lee et al., 2017), electrode materials (Goldfarb et al., 2017), and environmental remediation (Dashti et al., 2023; Priyanka et al., 2023, 2024). Biochar is primarily made from organic waste streams, such as agricultural wastes (lignocellulosic biomass), municipal solid wastes and animal manure (Xue et al., 2022). Biochar possesses the potential to remove 2.6 $GtCO_2$-eq yr^{-1}, where 1.1 $GtCO_2$-eq yr^{-1} can be carried out below \$100 tCO_2^{-1} (Nabuurs et al., 2023). While recent meta-analyses on biochar indicate increased CO_2 and reduced N_2O, such studies were carried out in laboratory and greenhouse-based settings, as opposed to actual sampling in the field (real world conditions) (Kalu et al., 2022). Alternatively, they can be stored through sequestration, aligned with Carbon Dioxide Removal (CDR) practices (Belmont et al., 2021; Renforth et al., 2023). This process effectively removes CO_2, mitigating emissions from the decay and thermal conversion of organic waste, leading to an ongoing and significant reduction in atmospheric Greenhouse Gas (GHG) levels (Ayaz et al., 2021).

On the other hand, one of the most critical environmental issues impacting public health and well-being is water contamination by heavy metals (Shaheen et al., 2019). This phenomenon is primarily attributed to extensive mining operations, including tailings, underground mine water and leachates, particularly from the extraction of metals for electric vehicle (EV) batteries such as lithium, nickel, copper, and cobalt. (Zhang et al., 2023). Waste Electrical and Electronic Equipment (WEEE), often considered non-recyclable is one of the world's fastest-growing

* Corresponding author.
E-mail address: martin.taylor@hull.ac.uk (M.J. Taylor).

https://doi.org/10.1016/j.jenvman.2024.122558
Received 21 May 2024; Received in revised form 25 August 2024; Accepted 16 September 2024
Available online 19 September 2024

waste streams. Its volume is expected to rise as our consumer culture drives the disposal of more electronic devices (Andeobu et al., 2021; de Vries and Stoll, 2021). In 2019, the global production of WEEE was approximately ~53.5 million metric tons and it is expected to exceed ~75 million metric tons in the next decade (Gulshan et al., 2024).

Globally, landfilling is the most common method of managing WEEE waste. This includes electrical and electronic devices including circuitry, wiring, storage devices, and semiconductor materials. These components have various hazardous metals such as Cu, Cd, Cr, Mn, Ni, Co, Ta, W, Nd, Pb, and Al. The metals, subject to concentration, can be toxic in water and the ground, especially when ingested. Also present in higher value components are precious metals including Ag, Au and Pd, known for their conductivity capabilities, malleability and resistance to tarnishing. Collectively, WEEE often end up in landfill's acidic/basic environment and come into contact with rainwater and microbes, promoting the digestion of heavy metals into the aqueous phase, generating a leachate that causes contamination to soil and natural habitats (Balali-Mood et al., 2021; Chakraborty et al., 2022; Djedjibegovic et al., 2020; Mishra et al., 2019; Shrestha et al., 2021).

Among the metals mentioned above, Cu is a common transition metal abundant in nature. Due to its versatility and extensive use in industrial applications, it is recognized as a significant hazardous heavy metal in wastewater from these processes (Liu et al., 2023). To overcome the rapid rate of metal-based pollution, several methods have been developed and applied to remove Cu from drinking water and wastewater. These include membrane separation, ion exchange, electrochemistry techniques, chemical precipitation, adsorption, biosorption, bio-precipitation, and bio-mineralisation (Liu et al., 2023). Among these methods, adsorption, including physisorption and chemisorption, has been found to be the efficient, operable, and cost-effective method for aqueous phase Cu remediation. The adsorption efficiency of an adsorbent depends on the pore structure, specific surface area and functional groups on the adsorbent surface (Ambaye et al., 2020; Fahmi et al., 2018; Inyang et al., 2016). Adsorbents can be classified into categories based on the material composition: carbon-based adsorbents, natural mineral adsorbents, and natural polymer adsorbents (Koppula et al., 2022). However, carbon-based adsorbents, specifically biochars, due to their carbon removal credentials and high customisability, are becoming more widespread for heavy metal removal, promoted by high available specific surface area, a well-developed pore structure and thermal stability/regenerative natures (Liu et al., 2022).

Chen et al. (2011) investigated the adsorption of Cu (II) using biochars produced from hardwood and corn straw. The adsorption results were characterised by the Langmuir isotherm model, which revealed maximum adsorption capacities of 12.52 mg/g and 6.79 mg/g on the hardwood biochar and corn straw biochar, respectively. Regmi et al., reported that KOH pre-treated switchgrass biochar was a highly efficient adsorbent compared to commercially available powdered activated carbon for the removal of Cu from an aqueous phase (Regmi et al. (2012). The adsorption efficiency of the activated biochar is attributed to the presence of oxygen-containing surface hydroxyl functional groups (-OH). The use of KOH-activated biochar derived from brewers draff (spent grain from the brewing industry) for the removal of Cu from synthetic and soil solutions has been studied using a batch reactor (Trakal et al., 2014). The activation of biochar with 2 M KOH provided a subtle increase to the BET available surface area and pore volume to 11.6 m^2/g (increasing from 9.8 m^2/g) and 8.74 cm^3/g, respectively, resulting in an adsorption capacity of 10.3 mg/g compared to 8.77 mg/g of the raw biochar. The removal of aqueous Cu (II) has also been experimentally and numerically examined using biochars pyrolysed from anaerobically digested algae-dairy-manure slurry (DAS), following a similar KOH activation process (Ortega et al., 2022). This biochar exhibited an enhanced Cu (II) adsorption capacity of 50.71 mg/g, 3.36x greater than biochars produced without using KOH. Activated biochar derived from cactus fibres, following nitric acid oxidation, showed relatively high capacity and chemical affinity for Cu (II) ions at neutral pH due to the presence of surface carboxylic functional groups (Liu et al., 2023).

In this study, mesoporous sugarcane bagasse (SCB) derived biochars with controllable surface area and pore structures were charged with the removal of Cu (II) ions in the aqueous phase, across the pH range (2–10). Specifically, this work will probe the optimum extraction efficiency to ascertain if the produced family of biochars are applicable for emerging polluted systems (e.g. Cu containing leachates in landfill sites) or ancestral contaminated waters (e.g. closed/abandoned mining sites). The produced materials were then scrutinized for their operational emissions in the form of electricity requirements, as well as a techno-economic assessment to determine the cost of Cu removal vs the production cost of the optimised bagasse derived mesoporous biochar. The synthesised biochars were produced by varying the KOH concentration in solution to maximise K impregnation into the bagasse superstructure, prior to pyrolysis to establish a pH responsive, highly porous material. By modelling the adsorption capabilities of the structured biochars with Responsive Surface Methodology (RSM), the resulting solver deduced optimised biochar and Cu adsorption conditions. This material was subsequently produced and validated against the model to assess and confirm the overall RSM viability.

2. Experimental

2.1. Bagasse biochar synthesis

The SCB used for this study was sourced from North Africa. The feedstock was milled using a Retsch Grindomix GM 200 knife mill (10,000 rpm for 5 min) before being sieved using a Retsch AS200 vibratory sieve stack, where the <250 μm fraction was reclaimed for further use. Deionised water was used to leach the water-soluble inorganic components (10 g/L) for 24 h at room temperature, previous work has found that this pre-treatment does not alter the organic composition of lignocellulosic wastes, while some ash components require extended residence times to be successfully extracted (Priyanka et al., 2023, 2024; Taylor et al., 2020).

Six mixtures of SCB and potassium hydroxide (KOH, Fisher Scientific, Extra Pure, SLR, Pellets) were created using varying KOH-SCB mass ratios in deionised water (100 mL); 0.25, 0.5, 0.75, 1.0, 1.25 and 1.5. The KOH-SCB mixtures were sonicated using a Fisherbrand S-Series Heated Ultrasonic Bath for 3 h at 50 °C. During this time, base hydrolysis separated cellulose and hemicellulose from the lignin polymeric backbone, as well as impregnating K atoms into the SCB grains, acting as a sacrificial pore templating agent. The suspensions were then dried overnight at 105 °C using a Fisherbrand convection oven, resulting in a brownish-yellow cake. The impregnated SCB subsequently underwent pyrolysis at 800 °C in nitrogen (~60 mL/min) using an Elite tube furnace with a ramp rate of 5 °C/min and holding for 1 h to convert the SCB into biochar. After pyrolysis, the biochars were washed with acetone (Fisher Scientific, Analytical reagent grade, >99.8%), until washings ran colourless (liberating all surface-based bio-oil and tar molecules), before drying at 105 °C overnight. The biochar was then suspended in 100 mL aqueous 5 M HCl, and refluxed for 3 h. Afterwards, the biochar was separated and washed with deionised water and dried under *vacuo,* followed by further drying at 105 °C overnight. In addition to these materials, a biochar was produced in the absence of KOH impregnation and acid reflux at 800 °C as an 'inactivated' benchmarking adsorbent.

2.2. Materials characterisation

Proximate analysis of the raw bagasse feedstock was carried out using a LECO TGA 701 thermogravimetric analyser at a ~1.00 g scale where moisture, volatile matter, fixed carbon, and ash were measured. In the TGA, the sample was heated from ambient temperature to 107 °C at a rate of 3 °C/min under nitrogen. It was then held at 107 °C for 15

min to remove moisture. Next, the temperature was increased from 107 °C to 950 °C at a rate of 5 °C/min and held at 950 °C for 7 min to remove any volatile components. Subsequently, the sample was cooled to 600 °C. This was followed by an ashing phase in air from 600 °C to 750 °C at 3 °C/min before cooling to ambient temperature. Fixed carbon was calculated by subtracting the mass of ash, volatile matter and moisture from the sample mass before combustion. Ultimate analysis (carbon, hydrogen and nitrogen content) of the biomass feedstock was acquired using a LECO CHN628 analyser for sample sizes of 50–70 mg. Biochar ash loading was determined using a Mettler Toledo TGA/DSC 1 in air at 30 mL/min, with a ramp rate of 10 °C/min from room temperature to 750 °C, holding for 1 h. The morphology of biochar was examined using a Scanning Electron Microscopy (SEM, Zeiss EVO 60) at 10^{-2} Pa and an electron acceleration voltage of 20 kV. For high-contrast imaging, the samples were coated with Au. Brunauer-Emmett-Teller (BET) surface area and pore volume of the biochars were analysed at −196 °C using a Micrometrics TriStar porosimeter, prior to analysis the samples were degassed for 3 h at 110 °C under a nitrogen capillary feed. Powder X-ray Diffraction (PXRD) measurements were acquired using mono-chromated Cu Kα radiation (λ = 0.1542 nm) on a PANalytical Empyrean series 2 diffractometer. Subsequent analysis of the diffractograms was performed in HighScore Plus (2013, PANalytical B.V.) with the ICDD's PDF-2 2012 database. The organic functional groups in the biochar were identified using Nicolet iS5 Fourier Transform Infrared (FTIR) spectrophotometer fitted with a PIKE MIRacle single reflection horizontal diamond ATR accessory in the range from 600 to 4000 cm^{-1}.

2.3. Cu uptake experimentation and analysis

For the purposes of this study, we simulated the copper contamination of mine wastewater effluent from the weathering of exposed copper seams from flooded abandoned mines, and tailings through an initial 200 ppm stock solution of Cu (II) (copper sulfate pentahydrate, $CuSO_4 \bullet 5H_2O$, Honeywell, 98%) prepared in deionised water. The effects of pH on biochar Cu extraction efficacy were investigated by diluting the stock solution in 100 mL H_2O, creating a 20 ppm Cu (II) experimental solution. The solution was then charged with 5 mg of biochar and the resulting suspension was adjusted to different pH (2–10) at a constant temperature of 20 °C, stirred at 300 rpm. The pH of the solution was controlled using 0.2 M HCl and 0.2 M NaOH (Thermo Scientific, pellets, 98%). Samples of the solution were taken at different time intervals (0, 2, 5, 10, 15, 20, 30 min) to study the kinetics of Cu (II) adsorption. Dose experiments were conducted by mixing varying masses (1, 2, 3, 4, and 5 mg) of each of the produced biochars in the experimental solution at 20 °C, across the pH range and stirring speed mentioned.

The copper concentrations of the samples were measured using a GENESYS 180 UV–Vis Spectrophotometer through chelation using a 50% ethanol-water solution (absolute ethanol, Fisher Scientific, >99.8%) containing 5 mg mL^{-1} cuprizone (bis(cyclohexanone)oxaleihydrazone, Sigma Aldrich, >95%) which was produced at 50 °C to fully dissolve the cuprizone into solution. Copper-containing aliquots (0.5 mL) were pipetted directly into a 3 mL quartz cuvette before adding two drops of 0.2 M NaOH solution, regulating the sample to pH 8, minimising liquid losses, where the absorbance of the copper-cuprizone complex was found to be its highest (Böck et al., 2022). To chelate the samples, 2.5 mL of the cuprizone solution was added into the quartz cuvette before being shaken (inverted several times) and left to react stoppered for 5 min in a static environment at room temperature. After this, the samples were measured in the UV–Vis zone between wavelengths of 550 nm–650 nm, where the peak of the copper-cuprizone complex is present (635 nm) (Messori et al., 2007). The cuprizone solution used was prepared on the same day as the copper concentrations were measured, as cuprizone has been found to precipitate out of the solution within 24 h, rendering the solution useless.

2.4. Parametric modelling and optimisation of Cu (II) removal performance

The relationship of each parameter (i.e., pH and biochar-KOH dosage ratio) and their interactive effects on Cu (II) ion adsorption performance were modelled using the non-linear regression curve fitting analysis paired with Levenberg–Marquardt algorithm in MATLAB R2023b software. All the coefficients were generated via regression, and the experimental responses obtained were fitted to the factors using multiple nonlinear regressions. The quality of the developed model fitting, and the significance of each variable were further assessed by analysis of variance (ANOVA) and coefficient of determination (R^2). Numerical optimisation was carried out to optimise the independent parameters for Cu (II) adsorption performance using the Response Surface Methodology approach (RSM). Confirmatory runs were physically carried out with an optimised biochar with parameters deduced from the model. Copper extraction measurements were repeated in triplicate to validate the accuracy and reliability of the predicted responses generated.

2.5. Economics assessment

To determine whether the effluent treatment process defined in Section 2.1 is profitable, operational expenses (OPEX) including energy costs that were linked to the process were determined. These included operating times, the maximum capacities of the equipment as well as the general dynamics of the process with occasional interventions of quality control tasks. To maintain consistency with the proposed experimental setup in Section 2.3, energy requirements were calculated to produce 5 mg of biochar. Energy analyses were carried out on the process for each unit of operation, which assisted in the isolation of costs for specific processes. To represent the average United Kingdom grid mix, electricity emissions and costs were carried out from GHG conversion factors and electricity costs through 0.28 $kgCO_2eq/kWh^{-1}$ and 36.32 $/kWh. Apart from processes requiring heat, no other electricity inputs were required at this scale of the process (Technology Readiness Level 4). The costs to remove Cu (II) were carried out through taking the removal potential that was produced from the experiments, and applying costs based upon the configuration of pH, KOH: SCB ratio and biochar quantity. The cost of removing copper relates to the direct costing of the process which can be calculated based upon Equation (1). This particular value quantifies the cost for the process to remove 1 mg of Cu (II) directly from wastewater effluent, or as specified for this work earlier, copper contaminated mine wastewater effluent from the weathering of exposed copper seams from flooded abandoned mines and tailings.

$$\text{Cost}\left[\$\ \text{mgCu (II)}^{-1}\right] = \frac{\text{Process cost [\$]}}{\text{Cu (II) removal from effluent [mgCu (II)]}} \quad (1)$$

2.6. Biochar recyclability

The recyclability of the optimised biochar was studied by loading a 100 mL, 20 ppm experimental Cu (II) solution with 5 mg of biochar deduced from the model, stirred at 300 rpm. Samples were collected after 20 min and the biochar was recovered through gravitational filtration. The recovered biochar was then refluxed in 30 mL 5 M HCl solution for 30 min, creating a green solution, before being filtered and washed with deionised water. The biochar was washed until the washing ran colourless (~100 mL). This process was carried out six times to assess the sustainability and longevity of the biochar adsorbent.

3. Results and discussion

3.1. Biochar characterisation results

The textural properties of the biochars, specifically the available surface area, pore volume and diameter, are shown in Table 1. The data

Table 1
Textural properties of the produced biochars with respect to increasing KOH content.

m_{KOH}/m_{SCB}	KOH in solution (M)[a]	BET Surface Area ($m^2\ g^{-1}$)	Pore volume ($cm^3\ g^{-1}$)	Average pore diameter (nm)
0.00	–	11.98	0.01	15.45
0.25	0.09	655.31	0.17	4.30
0.50	0.18	618.86	0.14	5.30
0.75	0.27	687.15	0.15	5.20
1.00	0.36	1061.77	0.33	5.70
1.25	0.45	779.52	0.26	4.00
1.50	0.54	728.52	0.72	7.00

[a] The KOH solution concentration when using 2 g of SCB per blend.

also includes baseline biochar that has not been activated (0.00 m_{KOH}/m_{SCB}) where the available surface area was reported as 11.98 $m^2\ g^{-1}$ and possesses a very limited pore volume (0.01 $cm^3\ g^{-1}$), therefore it can be considered that this biochar is a relatively non-porous bulk material. Wider, Table 1 shows that varying the amount of KOH used in relation to the bagasse significantly impacted the morphological properties of the biochar. Results indicate that the average pore diameter and pore volume have positive correlations with the KOH to SCB ratio, increasing gradually as additional KOH was used. Likewise, this trend was followed with respect to available surface area up to a maxima, 1061.77 $m^2\ g^{-1}$ (1.00 m_{KOH}/m_{SCB}), an overall increase of 1.62x than 0.25 m_{KOH}/m_{SCB} (655.31 $m^2\ g^{-1}$). After this point the surface area values rapidly begin to decrease, where for 1.50 m_{KOH}/m_{SCB} the pore diameter was found to increase by 1.34x from the material with the highest available surface area. Also, it is evident that the biochars possess a mesoporous structure, as indicated by the observation of adsorption-desorption type IV isotherms for each biochar, as presented in Fig. S1. It was discussed in earlier work on wheat straw biochars that the rapid decrease in surface area can be attributed to a collapsing pore structure (Priyanka et al., 2024). This therefore has shown that there is a 'tipping point' between ratio 1.00 and 1.25, here the additional potassium impregnated into the structure has caused the individual pores to collapse into one other, producing larger void spaces. Increasing further with the 1.50 ratio the larger voids will begin to coalesce which can explain the sudden drop in available surface area. At the molar scale, although the mass ratios are similar, the actual concentration of KOH in solution is relatively low (Table 1), where ratios of 1.00, 1.25 and 1.50 are 0.356 M, 0.446 M and 0.535 M, respectively. This means that taking the solution past ~0.4 M is the knife-edge for structural collapse, this does highlight a reason as to why the work mentioned by Trakal et al., presents a biochar with a surface area comparable with the untreated material due to using a 2 M KOH solution (Trakal et al., 2014). For this work, it is believed that the indirect ultrasound used has assisted both the hydrolysis reaction and K impregnation into the bagasse structure, meaning the KOH is more effectively utilised, as opposed to simply mixing.

Based on the SEM images in Fig. 1, one can see that the relative amount of KOH used had a significant effect on the overall quality and uniformity of the porous structure in the biochar. Before the alkali pre-treatment, the KOH-free biochar shows a lack of any significant porous structures (Fig. 1a). Upon the introduction of KOH, nano-scale pores begin to form on the walls of the bagasse fibers (Fig. 1b). Concentrated sections of these pores form patches of delicate structures, which explains the higher specific surface area and volume when compared to the KOH-free biochar (Fig. 1c and d). As the amount of KOH increases, the size of these pore openings continue to develop, resulting in larger sections appearing as a honeycomb structure (Fig. 1d). These immense structures then begin to combine with one another as they expand when the amount of KOH used increases past 1.00. The SEM images show that further increasing the KOH content caused the pores to combine to such an extent that the walls of the structure begin to deteriorate, producing larger void spaces and non-uniform pore openings (Fig. 1f and g). This resulting structural collapse, as mentioned previously has caused the

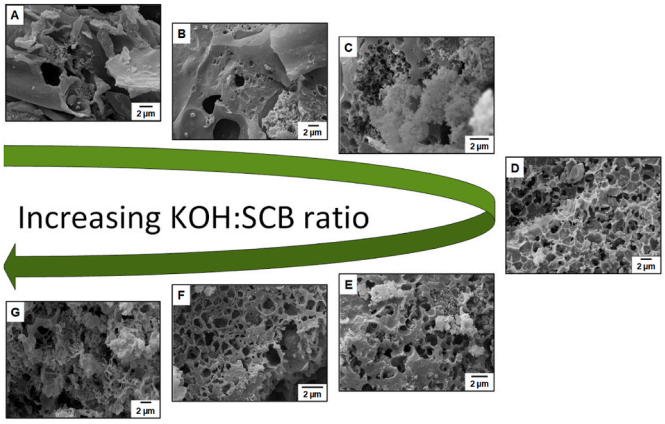

Fig. 1. SEM images of: **A)** 0.00 m_{KOH}/m_{SCB}, **B)** 0.25 m_{KOH}/m_{SCB}, **C)** 0.50 m_{KOH}/m_{SCB}, **D)** 0.75 m_{KOH}/m_{SCB}, **E)** 1.00 m_{KOH}/m_{SCB}, **F)** 1.25 m_{KOH}/m_{SCB} and **G)** 1.50 m_{KOH}/m_{SCB}.

sudden and consistent reduction in the surface area, observed in the porosimetry analysis with the increasing concentration of KOH used (Table 1).

Stacked FTIR spectra (Fig. 2a) of the biochars show that adding KOH has had a mild effect on the overall structure. However, an initial point to make is that all of the biochars show no broad -OH stretches due to their dry nature (highlighted by a marker at 3350 cm^{-1}). The peak seen for all pyrolysed biochar centered at 2100 cm^{-1} shows the presence of alkynes (Kończyk et al., 2022; Rodriguez et al., 2020) which have been recognized in the past to provide Lewis acidity (Priyanka et al., 2024). The smaller feature at 1990 cm^{-1} corresponds to the presence of allenes ($R_2C{=}C{=}CR_2$) within the structure, also known for exhibiting the same type of acidity and are known to be thermally induced (Chaudhary et al., 2023; Kończyk et al., 2022; Wijeyawardana et al., 2022). A peak at 1035 cm^{-1} was assigned to C-O stretching, commonly attributed to oxygenated structures in cellulose, hemicellulose, and lignin, this means that the pyrolysis has not removed all of the oxygen in the biochar (Domingues et al., 2017). However, this peak becomes stronger and shifts toward higher wavenumbers as KOH increases, therefore this stretch could be influenced by the reaction between the KOH and carbon superstructure. This could also be caused by the silica present in the biochar, as some researchers have reported that peaks centered between 1050 cm^{-1} and 1070 cm^{-1} can be attributed to Si-O stretching due to the high amount of silica present in SCB, highlighted by a yellow rectangle (Bachtiar et al., 2019; Cai et al., 2021; Lopez-Tenllado et al., 2021). There is logical agreement with this statement in the PXRD diffractograms, also shown in Fig. 2b, which show a variety of sharp crystalline features that can be indexed as silica. Finally, peaks at 937 cm^{-1} and 789 cm^{-1} also become more pronounced as KOH increases. These peaks can be attributed to aromatic C-H bending (Chen et al., 2014; Li et al., 2020; Zhang et al., 2011).

Additionally, for the PXRD diffractograms in Fig. 2b are two broad peaks centered at around 24.2° and 43.8° can be observed from the plot for all biochars. The initial signal is attributed to an amorphous entity due to how broad the shape is, whereas the signal at 43.8° has been denoted previously to turbostratic carbon (Ruz et al., 2016), as the biochar has some degree of order which bridges the gap between amorphous and crystalline graphite. This semi-ordering appears to not be promoted or prevented by the addition of KOH. Briefly mentioned in conjunction with the FTIR analysis, the jaggedness seen throughout the PXRD plots indicate the presence of nanoscale crystalline structures of silica scattered within the material, indexed as SiO_2. This rationale can be supported by the fact that SCB ash has been reported to contain >60% silica (Bachtiar et al., 2019). The Si species in the char are residues that remain from the parent bagasse feedstock, inorganic residues that were not removed during the leaching pre-treatment or through the

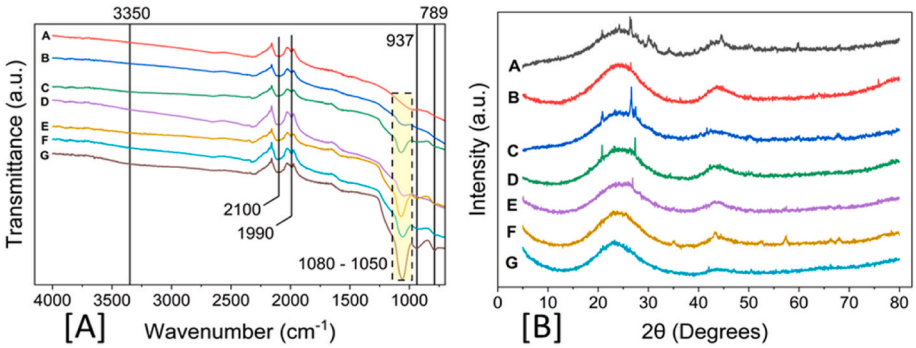

Fig. 2. FTIR **[A]** and PXRD **[B]** results: **A)** 0.00 m_{KOH}/m_{SCB}, **B)** 0.25 m_{KOH}/m_{SCB}, **C)** 0.5 m_{KOH}/m_{SCB}, **D)** 0.75 m_{KOH}/m_{SCB}, **E)** 1 m_{KOH}/m_{SCB}, **F)** 1.25 m_{KOH}/m_{SCB}, **G)** 1.5 m_{KOH}/m_{SCB}.

post-processing acid reflux. The intensity of these features was found not to be homogenous between samples, as is expected with the variability of lignocellulosic biomass waste. Silicon-based reflections are clearly shown in Fig. 2b in A, B, C, D, and E, where the most prominent feature at 26.5° is attributed to Si (111).

Deeper into the textural analysis to expand on from the FTIR and PXRD data, the ultimate analysis (CHN) of the biochars synthesised are shown in Table 2. It was found that the carbon content decreases at higher KOH ratios, this follows previously established rational that shows that the KOH reacts with surface carbon and generates K_2CO_3 (Dehkhoda et al., 2016; Fu et al., 2019; Priyanka et al., 2024). This goes on to react further with the carbon matrix when at temperature (pyrolysis), evolving CO into the gas phase and free K atoms which are impregnated into the lignocellulosic structure. The K_2CO_3 also decomposes to K_2O while evolving CO_2, while the remaining K_2O will react with carbon to generate free K atoms and CO into the gas phase. Therefore, it is expected that the KOH will etch away the carbon when establishing the pore network in the end product, the carbon in question will be removed into the gas phase. As the mesoporous materials will have a lower carbon content, it will inversely possess a higher ash content purely as a balance and not as a physical increase.

3.2. Cu uptake studies

3.2.1. Effects of pH and biochar structure variation

The effects of solution pH on copper adsorption for all biochars are shown in Fig. 3a and Fig. 3b, this demonstrates the preferential operating conditions for the biochars. In real world conditions, if considering a landfill site, a low pH is often aligned with a 'new' site and a high pH is linked with older, more established landfill sites. Mine tailings can be variable depending on additional ions present, such as carbonates. However, mines water can possess very low pH due to the presence of sulphides. Based on experiments, the 1.00 m_{KOH}/m_{SCB} biochar had the highest copper absorbance, across all pH investigated. However, the disparity between the 1.00, 1.25, and 1.50 m_{KOH}/m_{SCB} biochar is relatively small, when operating at pH 10 (Fig. 3a). Results also show that the baseline, bulk biochar (no KOH activation, 0.00 m_{KOH}/m_{SCB}) does not present a strong affinity for Cu (II) adsorption, across the full pH range studied, as compared with the KOH activated equivalent biochars. The superior performance of the 1:1 biochar (1.00 m_{KOH}/m_{SCB}) is attributed to its higher surface area, allowing Cu ions to bind to its free surface and developed pore network. A study conducted by Tan et al., has shown that biochar has negatively charged surfaces, which promote the adsorption of positively charged Cu (II) (Tan et al., 2020). It was found that the higher the biochar surface area, the more negatively charged active sites are present, which, in turn, would increase the capacity of Cu ions adsorbed by the biochar. Alternatively, the performance of the 1.00 m_{KOH}/m_{SCB} biochar can be attributed to the negative charge of its surface caused by oxygen-containing functional groups, such as that seen at 1035 cm^{-1} (C-O) in the FTIR spectra (Fig. 2) (Tan et al., 2020). Considering that Cu ions have a positive charge, the more negatively charged sites present in the biochar (charge characteristic dispersion with respect to increasing available surface area), the greater the Cu (II) concentration that can be adsorbed onto the surface. It is also logical to assume that water derived surface hydroxyls will also play a role in Cu uptake through ion exchange (Fig. 3c). Here, the water will adsorb to the surface due to biochar possessing a very hygroscopic nature. Again, with respect to a greater surface area and number of pores, the 1.00, 1.25 and 1.50 m_{KOH}/m_{SCB} materials demonstrate higher Cu extraction (Fig. 3b).

Similarly, one reason for the decrease in Cu (II) adsorption for m_{KOH}/m_{SCB} ratios of 1.25 and 1.50 is the ash content of the biochar, due to the further removal of available carbon units during the KOH treatment. Bagasse ash can contain metallic compounds such as calcium, magnesium, silicon and aluminium, which are positively charged (Herath et al., 2021). The increase in isolated positive characteristics (ash is not homogenous in biomass waste) can counteract or overcome the surface negative nature of the carbon matrix, especially if less carbon is available to generate surface hydroxyls.

The results from the adsorption experiments shown in Fig. 3a and Fig. 3b indicate that the biochar adsorbance increases with pH, therefore validating that the mesoporous biochars derived from bagasse are more suited to ancestral/established landfill sites and mine waters low in sulphides/high in carbonates. A previous study has shown that the zeta potential of the biochar's surface follows a downward trend with the increase of solution pH, suggesting that the surface charge of the biochar becomes much more negative in basic solutions (Tan et al., 2020). The more negative the surface becomes, the greater the interaction between the biochar surface and the Cu ions dispersed in solution, this authenticates the increased capacity in biochar adsorbance. Kang et al., found that Cu (II) adsorption on sludge derived biochar exhibited a similar behaviour (Kang et al., 2022). They observed that as the solution's pH increased, the adsorption capacity of biochar for Cu (II) also increased. This was due to the biochar's surface becoming more negatively charged, which created an electrostatic attraction with Cu (II) (Jiang et al., 2016). They also noted that under low pH conditions, H^+ in water outcompetes Cu (II) for the active sites on the biochar, leading to less

Table 2
Elemental analysis of the full range of bulk and mesoporous biochars produced.

m_{KOH}/m_{SCB}	C (wt%)	H (wt%)	N (wt%)	Ash (wt%)
0.00	62.97	0.91	0.52	22.99
0.25	57.43	1.90	0.25	17.32
0.50	53.32	2.30	0.17	19.66
0.75	51.73	2.44	0.16	21.01
1.00	44.60	2.43	0.24	24.56
1.25	47.02	1.66	0.23	35.42
1.50	29.22	1.19	0.12	46.64

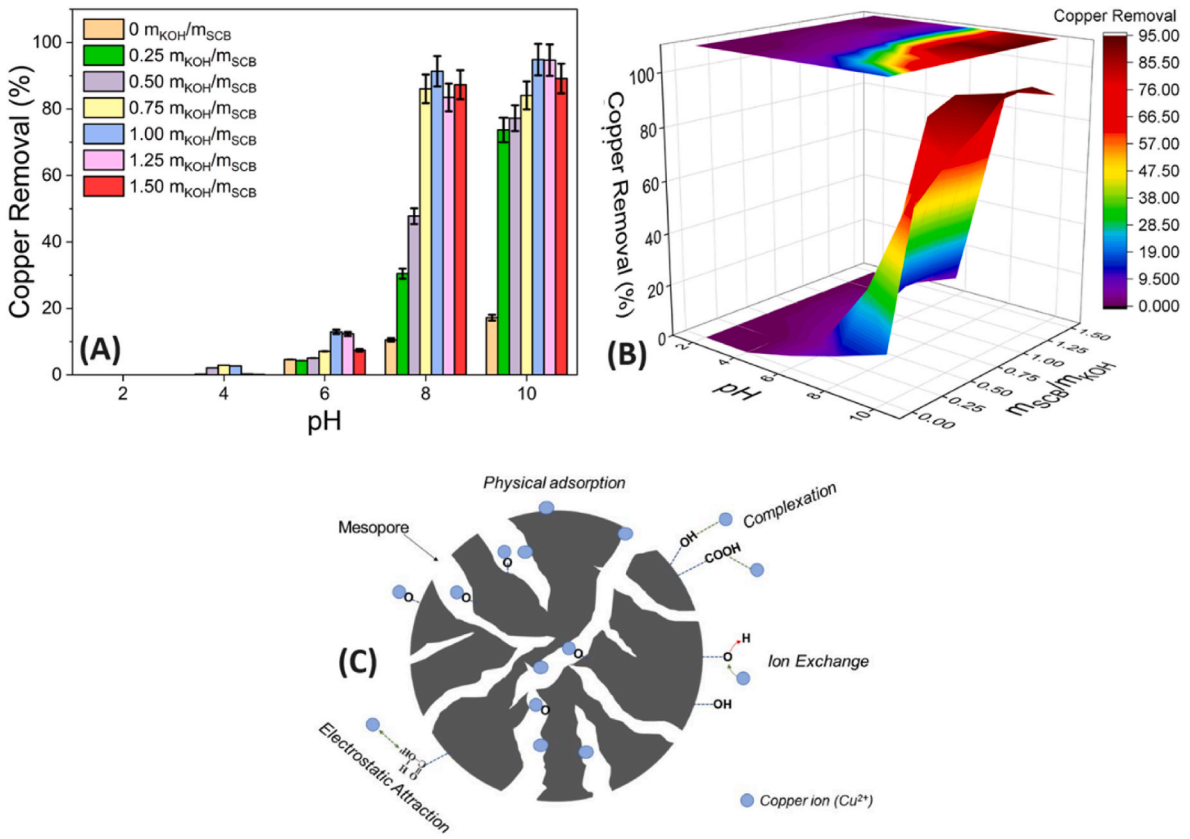

Fig. 3. (A) bar graph and (B) contour plot showing the effects of solution pH on percentage Cu (II) removal of 5 mg biochar, and (C) the possible Cu extraction mechanisms operating on/in the SCB derived biochar. Error bars represent ±5% error in measurement, as determined through triplicate analysis.

effective adsorption of Cu (II) on biochar (Pellera et al., 2012). Another study, (Yang et al., 2019), confirmed that the removal rate of Cu (II) by the Enteromorpha-derived biochar increased with increasing pH from 2.3 to 8.1. Regmi et al., reported that the removal efficiency of Cu (II) on the KOH-activated switchgrass-derived biochar dramatically increased as the pH was increased from 2.0 to 5.0 (Regmi et al., 2012). The removal efficiency remained around 100% at pH values of 5.0 and 7.0 but slightly decreased at pH 10.0. The reduction in the adsorption efficiency is attributed to the formation of insoluble Cu (II) precipitates, such as $Cu(OH)_2$, on the biochar surfaces as the pH increases above 10.0, hindering reduction and complexation reactions (Hoslett et al., 2019).

Possible Cu extraction mechanisms at play are shown in Fig. 3c, presented as physical adsorption, electrostatics (through the surface negative charge), pore filling, possible surface complexation with adsorbed hydroxyls from the water and ion exchange facilitated through the pH variation.

3.2.2. *Effects of Biochar dose*

Fig. 4 shows the effect of biochar dose on the Cu uptake experiments, conducted at the optimised reaction condition, pH 10. It was found that there is a steady increase in Cu (II) removal with increase dosage. This data only considers the KOH activated biochars as the unactivated biochar was found to be ineffective for Cu (II) adsorption. However, it can be noted that at 5 mg, the performance of the 1.00 and 1.25 m_{KOH}/m_{SCB} biochar becomes idle, suggesting that there is no further beneficial effect of increasing the biochar dose past 5 mg when operating at 20 ppm, in terms of cost and environment benefits.

3.2.3. *Adsorption kinetics models*

The Cu (II) adsorption kinetics were modelled using three equations to properly understand the adsorption kinetics: Pseudo-first order (P1O), pseudo-second order (P2O), and the Elovich model shown in the

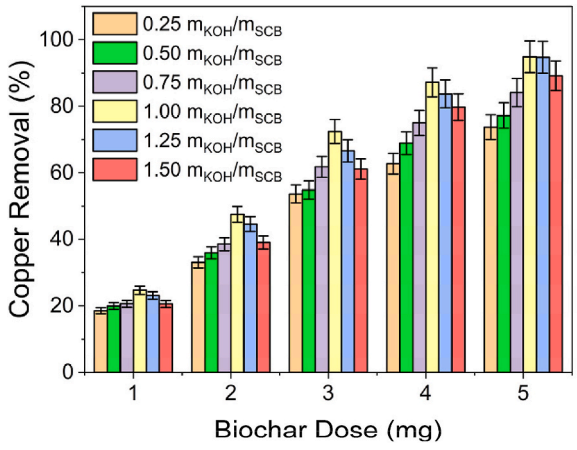

Fig. 4. The percentage of Cu ions removal for all biochar at varying doses at the pH 10, across 1–5 mg for a 20 ppm solution. Error bars represent ±5% error in measurement, as determined through triplicate analysis.

electronic supplementary information (ESI) as **Equation S(1), Equation S(2),** and **Equation S(3),** respectively. Where q_t and q_{eq} are the quantity of Cu (II) adsorbed by the biochar in mg g^{-1} at time t and equilibrium, respectively. k_1 and k_2 are equilibrium constants. And α and β are the initial adsorption rate and the Elovich constants in the experiment are defined in units of mg g^{-1} min^{-1} and g mg^{-1}, respectively (Wu et al., 2009).

P1O kinetics are generally observed when the rate of adsorption is limited by the bulk diffusion through the material (physisorption) (Bonelli et al., 2020). This could imply that the physical properties of the material, such as surface area, pore volume and physisorption, heavily

influence the rate of adsorption of the material. Meanwhile, P2O kinetics suggest that the rate-limiting factor of adsorption is the maximum or equilibrium capacity of the material used and not its quantity (chemisorption) (Bonelli et al., 2020). Lastly, the Elovich model describes an adsorbent with a heterogeneous surface (Wu et al., 2009). It suggests that adsorbed ions within the material interact with one another and that the rate of adsorption decreases as more of the solute is adsorbed within the material (Largitte and Pasquier, 2016). These kinetic models were used to understand the phenomenon governing the adsorption of Cu (II) ions. However, it should be noted that these models are not mutually exclusive. A study published by Ho and McKay has shown that some kinetic phenomena happen simultaneously, while others seem to transition to a different order of kinetics during their experiments (Ho and McKay, 1999).

The kinetics data (Fig. S2) shows that the quantity of Cu ions correlates positively with residence time, regardless of the types of biochar used. It can also be noted that there was a rapid uptake of copper within the initial 5 min, before it starts to plateau. These phases can be characterised as the initial fast adsorption and the slow adsorption phases, which were observed in similar studies (Asuquo et al., 2017; Ding et al., 2014). Researchers indicated that this behaviour is due to the availability of active adsorption sites on and within the adsorbent. The initial fast adsorption is due to fresh, unused sites where Cu ions can be adsorbed. As these sites become occupied, the rate of adsorption decreases (Asuquo et al., 2017). Table S1 presents the statistical analyses of the models used to fit the kinetics data, applying the pseudo first order (P1O, physisorption), pseudo second order (P2O, chemisorption) and Elovich models. Based on the data, it appears that all three models can be applied with a strong fit ($r^2 = 0.94–0.99$), although the P1O was not as applicable to the 0.25, 0.50 and 0.75 m_{KOH}/m_{SCB} biochars. Whereas the P2O and Elovich fit more consistently with the data, with only minor deviations due to variation in datapoints attributed to experimental error. It could be inferred that both physisorption and chemisorption adsorption mechanism are at play, agreeing with the proposed routes shown in Fig. 3c. However, it can be observed that the P2O kinetic model fits the behaviour slightly more consistently with the data (Fig. S2). Therefore, suggesting that chemisorption is the more favourable route for Cu (II) extraction when using mesoporous biochars, agreeing with interactions between surface hydroxyl groups opposed to directly adsorbing on/into to the carbon superstructure. The data in Table S1 shows that for both P1O and P2O, there was an increase in physical Cu (II) uptake with calculated values up to 371.395 mg/g and 389.835 mg/g for the 1.00 m_{KOH}/m_{SCB} biochar, respectively. As expected, the biochars with the lower surface areas exhibit poorer performance. This data also agrees with Fig. 3a, Fig. 3b and Fig. 4 that suggest the 1.00 and 1.25 m_{KOH}/m_{SCB} biochars operate very close to one another. From the P2O kinetic data, it was calculated that the physical uptake (qe) for these two materials was 389.835 mg/g and 383.565 mg/g, respectively. Although this shows a decrease, aligning with the overall narrative that surface area facilitates improved adsorption capabilities. Overall, there is a beneficial increase in Cu (II) uptake of 1.15x (52.371 mg/g) between 1.00 and 0.25 m_{KOH}/m_{SCB}.

4. Parametric modelling and optimisation of Cu(II) removal performance

The relationship of pH and biochar-KOH dosage ratio to the Cu (II) ion adsorption performance of the synthesised bagasse derived biochar was further investigated, confirmed, and optimised using a mathematical and statistical technique, namely Response Surface Methodology (RSM). The maximum Cu (II) adsorption capacity of sugarcane bagasse derived biochar was also obtained and evaluated under the analysis of variance (ANOVA). In this work, RSM, superimposed with Central Composite Rotatable Designs (CCRD), was selected as the design of experiments due to its inherent orthogonality and rotatability features, which reduces the full number of experimental runs required and significantly improves the variability of the multifactor studies without compromising the accuracy and reliability of the model experiments (Cheah et al., 2019). By doing so, modelling the full scenario to showcase the effects of pH conditions not completed experimentally and the performance of m_{KOH}/m_{SCB} ratios not physically produced is possible.

The relationship of each independent variable was presented and illustrated graphically in a three-dimensional space and contour plot, as shown in Fig. 5. Both independent variable responses were statistically correlated and fitted into a polynomial regression empirical model using MATLAB software. The final empirical equation of the model in terms of the coded factors is represented in **Equation (2)**:

$$\text{Cu (II) Removal Performance (\%)} = \left[6.71A\text{-}2.83A^2 + \frac{8.80}{1+\exp^{-1.71(B\text{-}6.62)}}\text{-}2.78\right]^2 \quad (2)$$

Where the coefficients A and B represent the biochar-KOH ratio and effect of pH, respectively. The coefficients with two factors, A^2 represents the quadratic effect of biochar-KOH ratio parameter. The negative sign in front of the term indicates an antagonistic effect, whereas the positive sign indicates a synergistic effect.

From the results, it showed that the mathematical model fits the experimental data very well with a correlation coefficient (R^2) of 0.9756. This is very close to unity and indicates the excellent fit quality of the regression model, and the ability of the model to confidently predict the adsorption capacity accurately. In other words, the regression model obtained can explain at least 98% of the variability in the predicted responses, and only <2% of the total variances was unable to be explained by the models. Moreover, the R^2 value was found to be in reasonable agreement with the adjusted R^2 value. Both the Mean Absolute Error (MAE, 3.9311) and Root Mean Square Error (RMSE, 6.7803) metrics also demonstrated a high degree of consistency between model predictions and experimental observations, reinforcing the model's robust performance. Additionally, the Nash-Sutcliffe Efficiency (NSE) of 0.9756, which is close to unity, further supports the quality of the fit by evaluating the relative magnitude of residual variance compared to the measured data. The equations used for this statistical analysis are denoted as **Equation S(4)**, **Equation S(5)** and **Equation S(6)** in the ESI. In the context of independent variable statistical significance, it was found that the biochar-KOH ratio appeared to be the only significant linear factor, with a P-value less than 0.05%. On the other hand, the effect of pH was revealed to exhibit a sigmoidal effect towards copper removal. There was no significant interactive effect between the pH or biochar-KOH ratio to the Cu (II) adsorption performance. However, the quadratic effect of the biochar-KOH ratio was the only interaction term found to be significant in affecting the Cu (II) adsorption performance.

To access accuracy of the empirical model, the predicted versus measured Cu removal results were plotted in Fig. S3. Taking into all performance results, a good accordance between the model prediction and measured experimental data were revealed in Fig. S3a, whereby they fitted the linear line well, with a confidence of $R^2 = 0.993$ and a slope of 0.9968 that is very close to unity. This implied that the model prediction could quantify the performance of the observed Cu removal with sufficient accuracy. To further evaluate the applicability of the

Model Name	Copper Removal (%)
Equation	$\left[AX + BX^2 + \frac{C}{1 + exp(D(Y - E))} + F\right]^2$
A	6.79253 ± 0.05108
B	-2.8820 ± 0.02762
C	8.79634 ± 0.04109
D	-1.72055 ± 0.0113
E	6.6179 ± 0.00974
F	-2.81353 ± 0.04485
Reduced Chi-Square	0.06897
R-Square (COD)	0.99996
Adjusted R-Square	0.99995
RMSE	6.7803
MAE	3.9311
NSE	0.9756

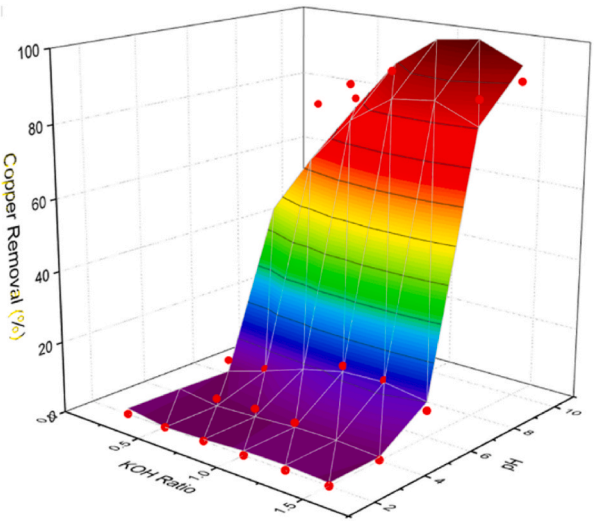

Fig. 5. 3D response surface plot and ANOVA table for Cu (II) adsorption of mesoporous biochars.

developed model at different operating conditions, the prediction and measured experimental data were charted in Fig. S3b. It was seen that at different biochar-KOH ratio, the model prediction and actual measured data at varying pH were in agreement, which were demonstrated via linear correlation with slope and R^2 consistently close to 1. The only exception was at biochar-KOH ratio of 1:0.25 in which a comparatively deviated slope and correlation fit from unity were observed, that might be attributed to the low concentration of KOH that was not sufficient to induce the alkaline promoted effect for the biochar. It was reported that the presence of sufficient alkaline could potentially clear the biochar pores. This could also promote metal stabilization during the immobilization process, but to a certain extent since high alkalization can result in the swelling of the intrinsic lignin structure of the biochar (Wang et al., 2020). At a low biochar-KOH ratio of 1:0.25, the promoted alkaline effect was comparatively less significant, and hence not sufficiently captured by the model that incorporated both the impacts of pH and KOH concentration towards Cu (II) removal.

At a confidence level of 95%, the predicted maximum adsorption capacity was calculated to be 99.20%, at the optimal pH 10 and an adsorbent created from biochar-KOH ratio of 1.18. To further validate the accuracy and reliability of the model engendered by the circumscribed CCRD, three confirmatory runs were carried out in parallel, utilising a biochar produced at a ratio of 1.18, as directed by the model, under the optimum conditions (textural properties of the 1.18 material are found in Table S2). It was found that the Cu (II) removal performance of the 1.18 m_{KOH}/m_{SCB} biochar was in close alignment with the predicted value of 99.20% with an experimental removal of 97.85%, as indicated in Fig. 6a. This is a deviation of 1.35% between the theoretical and experimental data. This confirms the optimum reaction conditions predicted by the numerical regression model in yielding reproducible experimental data, which strengthened the reliability of the empirical model. Further validation of the relationship between experimental data and the empirical model is shown in Fig. 6b. The relationship begins to align from 0.50 m_{KOH}/m_{SCB} and remains a strong fit for the following biochars. The textural properties of the 1.18 m_{KOH}/m_{SCB} biochar are found in Table S2, this data shows that the available surface area increased subtly compared with the 1.00 m_{KOH}/m_{SCB} biochar (1073.85 $m^2\ g^{-1}$ vs 1061.77 $m^2\ g^{-1}$). As expected, the carbon content in the biochar was lower as a higher KOH concentration was used during material synthesis.

5. Techno-economic analysis (TEA)

To assess the true value in use of an activated, mesoporous biochar, one must consider the cost analysis from cradle-to-grave or otherwise considered the production cost itself. This includes materials and input

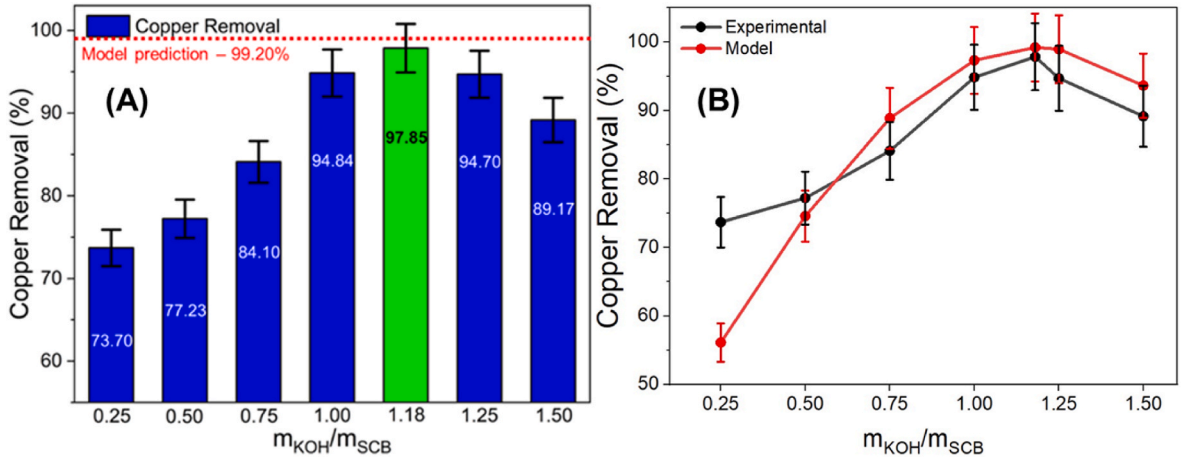

Fig. 6. (a) Copper removal of all biochars at ideal conditions (5 mg biochar, pH 10) superimposed with the predicted copper removal (dashed line). (b) presents the overall relationship between the experimental data and the optimised model. Error bars represent ±5% error in measurement, as determined through triplicate analysis.

energy costs, while highlighting the emissions abatement and revenue of reclaimed Cu (II), depending on salt produced.

Currently, the average cost of sugarcane is between $1.38-$3.45/kg (Wamucii, 2024). For every tonne of sugarcane extracted, approximately 280 kg of sugarcane bagasse is recovered, (Cerqueira et al., 2007) and sugarcane production is expected to grow by 1% every year up to 2 Gt by 2030 (560 Mt of sugarcane bagasse produced) (OECD., 2019). potentially increasing further in areas such as Brazil and India, which have previously reported to produce 46.3% of the world's production value (Heniegal et al., 2020). According to (Moran, 2018), the average density of wastewater was 1400 kg/m^3. Global wastewater production has been estimated to be around 503 trillion litres, of which 63% (317 trillion litres) is collected, 48% (262 trillion tonnes) is treated and 53% (242 trillion tonnes) is left untreated (Jones et al., 2021). The average Cu (II) concentration found in wastewater is assumed to be 2.5–10,000 mg/L (Liu et al., 2023), indicating that at least 604 Mt of Cu (II) may be present in wastewater alone. The results of the techno-economic analysis are presented in Table 3. The cost of 5 g of raw biochar materials using KOH at different ratios was between $0-$1.5. The total cost of removing 1 mg Cu (II) in the best-case scenario (1.18 mKOH/mSCB biochar, as directed by the RSM data and validated experimentally) reached $4.08/mgCu(II)$^{-1}$ removed. This value includes all raw materials, processing mediums (nitrogen and deionised water), purification and post-treatment chemicals (acetone and HCl), as well as energy input steps such as sonication, drying and the core pyrolysis process. Energy prices for electrical inputs were taken from local sources. Table 3 also shows the impact on cost through the salt recovered post extraction, including chemically washing the biochar post uptake. However, this physical Cu removal from the biochar was not factored into the end point cost, only the uptake itself. The data clearly shows that reclaiming the Cu (II) in the chloride form is the most cost-effective approach, where the sulfate salt is the most cost negative. The method proposed in this study is compared with a range of others using alternative materials, uptake conditions and scalability in Table S3. The methods shown in Table S3 are also compared with the projected cost of removal in this work, using the values in Table 3, as well as current costs for materials and reagents to estimate alternative costs of Cu (II) removal. Key takeaways from the various technologies are that the method proposed in this study appears to be more cost-effective than some methods of membrane filtration ($8–15/mg Cu (II)), biosorption ($3–7/mg Cu (II)), solvent extraction ($5–10/mg Cu (II)), catalysis ($7–12/mg Cu (II)) and ion exchange ($6–12/mg Cu (II)). This work was also found to be more effective in terms of physical uptake than some forms of ion exchange, especially at high pH, chemical precipitation and solvent extraction. The only disadvantage identified was that the initial setup costs for this study are its limiting factor. This is mildly compounded as alternative methods mentioned are already available wildly, proving to not be as cost effective.

Table 3
Mass and energy costs for best-case scenario: 5 g biochar, 1.18 KOH ratio and 97.85% Cu (II) removal.

Raw materials and prices			
Inventory	Unit Price ($)	Dosage	Cost ($ mg Cu (II)$^{-1}$ removed)
Makeup chemicals			
SCB	0.67/kg	5 g	$8.56x10^{-3}$
KOH	49.59/500 g	0–1.5	0.613
Deionised water	0.03/L	5 L	$8.07x10^{-2}$
N_2	0.64/L	2.5 L	0.825
Quality control			
Acetone	22.09/L	0.5 mL	$2.82x10^{-2}$
HCl	26.16/500 g	0.5 mL	$6.68x10^{-2}$
Electricity			
Ultrasonic bath	0.36/kWh	0.285 kWh	0.526
Drying (Overnight)	0.36/kWh	0.6 kWh	0.110
Pyrolysis (Furnace)	0.36/kWh	10.28 kWh	1.91
Revenue			
Recover as $CuCl_2$	14.64/250 g	1 mg	$-1.46x10^{-4}$
Recover as $CuSO_4$	29.21/100 g	1 mg	$-7.26x10^{-4}$
Recover as $Cu(NO_3)_2$	12.20/100 g	1 mg	$-3.03x10^{-4}$

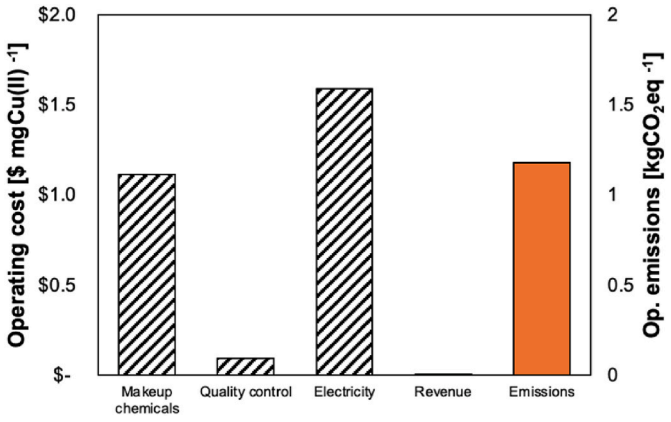

Fig. 7. Techno-economic performance per mg Cu (II) adsorption.

Assessing the economic performance of biochar always provides a unique and interesting perspective, mainly due to the sheer variety of different biochar pathways and applications. Fig. 7 illustrates the results of the TEA with a KOH: SCB ratio of 1.18, the modified biochar was found to remove 97.85% Cu (II), within laboratory conditions, presenting a Technology Readiness Level (TRL) 4. Despite the high removal rate, techno-economics are necessary to ensure that the process is optimised for future scale-up to higher TRL levels (pilot scale and beyond), identifying hotspots within key production processes, and ultimately minimising costs. Fig. 7 shows that the major cost concern is related to the input electricity cost, followed by the 'makeup chemicals' (KOH and nitrogen). However, subject to electricity cost, depending on production route and location, this could prove to be lower, as well as the nitrogen used for the pyrolysis originating from a generator (increasing electricity cost) or other means.

Table 4 highlights the adsorbent dose, pH, Cu (II) concentration, adsorption capacity and ultimately, the removal efficiency of various modified biochars within the wider literature, comparing finally with the optimised material produced in this study. Most Cu (II) concentrations within the literature occur at levels that reflect what would be found in wastewater and effluent, with the median concentration at approximately 50 mg/L.

The adsorbent dose for example, removes most of the Cu (II) when the range is around 5 g/L, consistent with the results performed in this study. The best removal rates in these studies also tend to occur at slightly acidic conditions with median pH levels of around 5–6. This observation goes against the trends observed in this study, where the highest removal rates are achieved at pH 10 for example. This therefore shows that the mesoporous biochars produced in this study are more suited for established landfill sites and basic mine waters. In acidic conditions, these materials were outperformed by a number of alternative materials presented in Table 4. However, due to the available surface area and porosity of the biochars in this work, a much lower dose could be used per charge to achieve comparable/superior uptake characteristics.

6. Biochar recyclability results

Fig. S4 shows the results of the recyclability experiment for the optimised biochar (1.18 mKOH/mSCB) at pH 10. The adsorbent cycles

Table 4
Maximum Cu (II) removal efficiency from other biochar studies.

Adsorbent	Adsorbent dose (g/L)	pH	Cu (II) concentration (mg/L)	Adsorption capacity (mg/g)	Max. Removal efficiency (%)	Reference
Hardwood	1–50	7	63	6.8	56.7	Chen et al. (2011)
Corn straw	1–50	5	63	12.5	98.3	
Peanut straw	2	5	157–790	89	78.2	Tong et al. (2011)
Soybean straw	2	5	157–790	52.7	78.2	Tong et al. (2011)
Canola Straw	2	5	157–790	37.5	78.2	Tong et al. (2011)
Treated pig manure	5	5	6.3–157	6.8	87.2	Kołodyńska et al. (2012)
Switchgrass vs hydrothermal carbonisation	2	5	40	4	99.9	Regmi et al. (2012)
Rice husks (hydrothermal)	5–12.5	5–6	20–50	1.09	90.1	Pellera et al. (2012)
Rice husks (pyrolysis)	5–12.5	5–6	20–50	0.02–2.9	90.1	Pellera et al. (2012)
Olive pomace (hydrothermal)	5–12.5	5–6	20–50	0.6	77.8	Pellera et al. (2012)
Olive pomace (pyrolysis)	5–12.5	5–6	20–50	0.17–1.3	77.8	Pellera et al. (2012)
Orange waste (hydrothermal)	5–12.5	5–6	20–50	2.03	88.7	Pellera et al. (2012)
Orange waste (pyrolysis)	5–12.5	5–6	20–50	0.08–1.4	88.7	Pellera et al. (2012)
Compost (hydrothermal)	5–12.5	5–6	20–50	3.8	93.6	Pellera et al. (2012)
Compost (Pyrolysis)	5–12.5	5–6	20–50	2.4–3.6	93.6	Pellera et al. (2012)
Spartina alterniflor	2.3	6	50–290	48.5	48.5	Li et al. (2013)
Dairy manure	N/A	5.18–6.98	317	54.4	62.4	Xu et al. (2013)
Peanut straw	20	5.88	773.61	N/A	98.0	Tong and Xu (2013)
Canola straw	20	7.17	773.61	N/A	97.1	Tong and Xu (2013)
Soybean straw	20	7.51	773.61	N/A	94.1	Tong and Xu (2013)
Rice straw	20	5.0	773.61	N/A	88.4	Tong and Xu (2013)
Rice Husk	0.1–1	1.5–4	100–500	20.83	74.5	Elhafez et al. (2017)
Paper mill sludge	0.1–0.3	4–6	30	119.90	99.8	Xu et al. (2021)
Sawdust (Various)	1–3	1.5–5.5	50–200	91.74–133.33	98.3	Elhafez et al. (2017)
Sugarcane Bagasse	1–5	10	20	1.95	97.85	This study

1–3 show a gradual loss in effectiveness from 97% to 88%, assuming an average loss of 3% each cycle. However, there was a larger decrease shown for cycles 4 and 6 which are attributed to biochar losses through transfers, regeneration and washing. As the test utilised 5 mg of adsorbent, it is clear that the same mass of material could not be sustained for the full investigation. This being said, even after six cycles and losses from the initial 5 mg, the biochar was still effective showing a Cu (II) removal of 64%. Following Fig. 4, it could be inferred that the remaining biochar in solution was ~2.5 mg due to presenting similar Cu (II) removal at pH 10, meaning that the biochar itself has long term reusability/sustainability.

7. Conclusions

Scalable and customizable mesoporous biochars derived from sugarcane bagasse were successfully developed in this study. By accommodating a biomass waste pre-treatment process (KOH impregnation via sonication), followed by post pyrolysis processing (refluxing in HCl), the biochar produced utilising a 1:1 ratio of feedstock and KOH presented an available surface area of 1061.77 m^2 g^{-1}. However, upon further inclusion of KOH, it was found that the pore structure began to collapse, diminishing the surface area. By interfacing these materials (5 mg) with a Cu (II) solution across a range of pH environments, it was found that the biochars with the highest surface areas were superior (1.00 m_{KOH}/m_{SCB} indicating a Cu (II) removal of 94.85%), specifically at pH 10, contrary to a swath of alternative biochars in the literature which favour acidic media. This work also demonstrates how a baseline, non-activated biochar is not appropriate for high Cu (II) removal. Further, the mesoporous biochar adsorbent technology developed and tested in this work has been estimated to operate at an overall lower cost for Cu (II) removal than alternative removal technologies such as; ion exchange, solvent extraction, membrane filtration, chemical precipitation and coagulation/flocculation. However, a disadvantage to this method is the initially high cost associated with biochar preparation compared with the well-established methods mentioned above. Other limitations of this study are the feedstock used itself, although not highly abundant globally, it is produced in large quantities in locations that also have active/decommissioned copper mines. As is understood in the literature and previous work, biochar activation is variable depending on the feedstock used, where higher available surface areas and pore structures have been found for cereal derived biochars. To determine the full capabilities of this range of bio-derived adsorbents, they were further investigated and optimised using a mathematical and statistical technique, namely Response Surface Methodology (RSM). The resulting model, produced from the experimental results, predicted the trend between the copper adsorbance versus the SCB-KOH ratio to a confidence of 95%. The model predicted that a 1.18 m_{KOH}/m_{SCB} biochar would exhibit a copper removal of 99.20%, when operating at pH 10. Experimental results validated this prediction by removing 97.85%, a deviation of 1.35%, confirmed via triplicate experimentation. Experiments also show that the biochar can be recycled over six times, presenting a subtle decrease in efficiency overtime. The largest decreases in recyclability using the biochars in this work are the physical transfer losses. This suggests that the biochars themselves maintain high sustainability.

CRediT authorship contribution statement

Julius G. Bongosia: Writing – review & editing, Writing – original draft, Methodology, Investigation, Formal analysis, Data curation. **Amthal Al-Gailani:** Writing – review & editing, Writing – original draft, Investigation, Conceptualization. **Ben W. Kolosz:** Writing – review & editing, Writing – original draft, Formal analysis, Data curation, Conceptualization. **Adrian Loy Chun Minh:** Writing – review & editing, Validation, Conceptualization. **Serene Sow Mun Lock:** Writing – review & editing, Writing – original draft, Formal analysis, Data curation. **Kin Wai Cheah:** Writing – review & editing, Writing – original draft, Investigation, Formal analysis, Data curation. **Martin J. Taylor:** Writing – review & editing, Supervision, Resources, Methodology, Investigation, Formal analysis, Conceptualization.

Declaration of competing interest

The authors declare that they have no known competing financial

interests or personal relationships that could have appeared to influence the work reported in this paper.

Data availability

Data will be made available on request.

Acknowledgements

We would like to thank Mr. Timothy Dunstan for the HRSEM images.

Appendix A. Supplementary data

Supplementary data to this article can be found online at https://doi.org/10.1016/j.jenvman.2024.122558.

References

Ambaye, T.G., Vaccari, M., van Hullebusch, E.D., Amrane, A., Rtimi, S., 2020. Mechanisms and adsorption capacities of biochar for the removal of organic and inorganic pollutants from industrial wastewater. Int. J. Environ. Sci. Technol. 18, 3273–3294.

Andeobu, L., Wibowo, S., Grandhi, S., 2021. A systematic review of E-waste generation and environmental management of asia pacific countries. Int. J. Environ. Res. Publ. Health 18, 9051.

Asuquo, E., Martin, A., Nzerem, P., Siperstein, F., Fan, X., 2017. Adsorption of Cd(II) and Pb(II) ions from aqueous solutions using mesoporous activated carbon adsorbent: equilibrium, kinetics and characterisation studies. J. Environ. Chem. Eng. 5, 679–698.

Ayaz, M., Feizienė, D., Tilvikienė, V., Akhtar, K., Stulpinaitė, U., Iqbal, R., 2021. Biochar role in the sustainability of agriculture and environment. Sustainability 13, 1330.

Bachtiar, E., Marzuki, I., Setiawan, A.M., Yunus, A.I., Gusty, S., 2019. Potency of Sugarcane bagasse ash partial subtitution of cement in concrete. First International Conference on Materials Engineering and Management-Engineering Section (ICMEMe 2018). Atlantis Press, pp. 27–31.

Balali-Mood, M., Naseri, K., Tahergorabi, Z., Khazdair, M.R., Sadeghi, M., 2021. Toxic mechanisms of five heavy metals: mercury, lead, chromium, cadmium, and arsenic. Front. Pharmacol. 12, 643972.

Belmont, E., Sanchez, D.L., Smith, P., Torn, M., 2021. The building blocks of CDR systems: geological sequestration. In: Wilcox, J., Kolosz, B., Freeman, J. (Eds.), Carbon Dioxide Removal Primer.

Böck, F.C., Helfer, G.A., da Costa, A.B., Dessuy, M.B., Ferrão, M.F., 2022. Low cost method for copper determination in sugarcane spirits using Photometrix UVC® embedded in smartphone. Food Chem. 367, 130669.

Bonelli, B., Freyria, F.S., Rossetti, I., Sethi, R., 2020. Nanomaterials for the Detection and Removal of Wastewater Pollutants. Elsevier.

Cai, T., Liu, X., Zhang, J., Tie, B., Lei, M., Wei, X., Peng, O., Du, H., 2021. Silicate-modified oiltea camellia shell-derived biochar: a novel and cost-effective sorbent for cadmium removal. J. Clean. Prod. 281, 125390.

Cerqueira, D.A., Filho, G.R., Meireles, C.d.S., 2007. Optimization of sugarcane bagasse cellulose acetylation. Carbohydrate Polymers 69, 579–582.

Chakraborty, S., Qamruzzaman, M., Zaman, M., Alam, M.M., Hossain, M.D., Pramanik, B., Nguyen, L., Nghiem, L., Ahmed, M., Zhou, J., 2022. Metals in e-waste: occurrence, fate, impacts and remediation technologies. Process Saf. Environ. Protect. 162, 230–252.

Chaudhary, H., Dinakaran, J., Vikram, K., Notup, T., Rao, K., 2023. Evaluation of physico-chemical and structural properties of biochar produced from pyrolysis of urban biowaste. J. Mater. Cycles Waste Manag. 25, 2845–2860.

Cheah, K.W., Yusup, S., Kyriakou, G., Ameen, M., Taylor, M.J., Nowakowski, D.J., Bridgwater, A.V., Uemura, Y., 2019. In-situ hydrogen generation from 1,2,3,4-tetrahydronaphthalene for catalytic conversion of oleic acid to diesel fuel hydrocarbons: parametric studies using Response Surface Methodology approach. Int. J. Hydrogen Energy 44, 20678–20689.

Chen, T., Zhang, Y., Wang, H., Lu, W., Zhou, Z., Zhang, Y., Ren, L., 2014. Influence of pyrolysis temperature on characteristics and heavy metal adsorptive performance of biochar derived from municipal sewage sludge. Bioresour. Technol. 164, 47–54.

Chen, X., Chen, G., Chen, L., Chen, Y., Lehmann, J., McBride, M.B., Hay, A.G., 2011. Adsorption of copper and zinc by biochars produced from pyrolysis of hardwood and corn straw in aqueous solution. Bioresour. Technol. 102, 8877–8884.

Dashti, A., Raji, M., Riasat Harami, H., Zhou, J.L., Asghari, M., 2023. Biochar performance evaluation for heavy metals removal from industrial wastewater based on machine learning: application for environmental protection. Separation and Purification Technology 312, 123399.

de Vries, A., Stoll, C., 2021. Bitcoin's growing e-waste problem. Resour. Conserv. Recycl. 175, 105901.

Dehkhoda, A.M., Gyenge, E., Ellis, N., 2016. A novel method to tailor the porous structure of KOH-activated biochar and its application in capacitive deionization and energy storage. Biomass Bioenergy 87, 107–121.

Ding, W., Dong, X., Ime, I.M., Gao, B., Ma, L.Q., 2014. Pyrolytic temperatures impact lead sorption mechanisms by bagasse biochars. Chemosphere 105, 68–74.

Djedjibegovic, J., Marjanovic, A., Tahirovic, D., Caklovica, K., Turalic, A., Lugusic, A., Omeragic, E., Sober, M., Caklovica, F., 2020. Heavy metals in commercial fish and seafood products and risk assessment in adult population in Bosnia and Herzegovina. Sci. Rep. 10, 13238.

Domingues, R.R., Trugilho, P.F., Silva, C.A., Melo, I.C.N.d., Melo, L.C., Magriotis, Z.M., Sanchez-Monedero, M.A., 2017. Properties of biochar derived from wood and high-nutrient biomasses with the aim of agronomic and environmental benefits. PLoS One 12, e0176884.

Elhafez, S.E.A., Hamad, H.A., Zaatout, A.A., Malash, G.F., 2017. Management of agricultural waste for removal of heavy metals from aqueous solution: adsorption behaviors, adsorption mechanisms, environmental protection, and techno-economic analysis. Environ. Sci. Pollut. Control Ser. 24, 1397–1415.

Fahmi, A.H., Samsuri, A.W., Jol, H., Singh, D., 2018. Physical modification of biochar to expose the inner pores and their functional groups to enhance lead adsorption. RSC Adv. 8, 38270–38280.

Fu, Y., Shen, Y., Zhang, Z., Ge, X., Chen, M., 2019. Activated bio-chars derived from rice husk via one- and two-step KOH-catalyzed pyrolysis for phenol adsorption. Sci. Total Environ. 646, 1567–1577.

Goldfarb, J.L., Dou, G., Salari, M., Grinstaff, M.W., 2017. Biomass-based fuels and activated carbon electrode materials: an integrated approach to green energy systems. ACS Sustain. Chem. Eng. 5, 3046–3054.

Gulshan, S., Shafaghat, H., Wang, S., Dai, L., Tang, C., Fu, W., Wen, Y., Wang, C.H., Evangelopoulos, P., Yang, W., 2024. Kinetic investigation on the catalytic pyrolysis of plastic fractions of waste electrical and electronic equipment (WEEE): a mathematical deconvolution approach. Waste Manag. 187, 156–166.

Guo, S., Li, Y., Wang, Y., Wang, L., Sun, Y., Liu, L., 2022. Recent advances in biochar-based adsorbents for CO2 capture. Carbon Capture Science & Technology, 100059.

Heniegal, A.M., Ramadan, M.A., Naguib, A., Agwa, I.S., 2020. Study on properties of clay brick incorporating sludge of water treatment plant and agriculture waste. Case Stud. Constr. Mater. 13.

Herath, A., Layne, C.A., Perez, F., Hassan, E.I.B., Pittman, C.U., Mlsna, T.E., 2021. KOH-activated high surface area Douglas Fir biochar for adsorbing aqueous Cr(VI), Pb(II) and Cd(II). Chemosphere 269, 128409.

Ho, Y.S., McKay, G., 1999. Pseudo-second order model for sorption processes. Process Biochemistry 34, 451–465.

Hoslett, J., Ghazal, H., Ahmad, D., Jouhara, H., 2019. Removal of copper ions from aqueous solution using low temperature biochar derived from the pyrolysis of municipal solid waste. Sci. Total Environ. 673, 777–789.

Inyang, M.I., Gao, B., Yao, Y., Xue, Y., Zimmerman, A., Mosa, A., Pullammanappallil, P., Ok, Y.S., Cao, X., 2016. A review of biochar as a low-cost adsorbent for aqueous heavy metal removal. Crit. Rev. Environ. Sci. Technol. 46, 406–433.

Jiang, S., Huang, L., Nguyen, T.A.H., Ok, Y.S., Rudolph, V., Yang, H., Zhang, D., 2016. Copper and zinc adsorption by softwood and hardwood biochars under elevated sulphate-induced salinity and acidic pH conditions. Chemosphere 142, 64–71.

Jones, E.R., van Vliet, M.T.H., Qadir, M., Bierkens, M.F.P., 2021. Country-level and gridded estimates of wastewater production, collection, treatment and reuse. Earth Syst. Sci. Data 13, 237–254.

Kalu, S., Kulmala, L., Zrim, J., Peltokangas, K., Tammeorg, P., Rasa, K., Kitzler, B., Pihlatie, M., Karhu, K., 2022. Potential of biochar to reduce greenhouse gas emissions and increase nitrogen use efficiency in boreal arable soils in the long-term. Front. Environ. Sci. 10.

Kang, X., Xiao, F., Zhou, S., Zhang, Q., Qiu, L., Wang, L., 2022. Study on the performance of sewage sludge biochar modified by nZVI to remove Cu(II) and Cr(VI) in water. Water Sci. Technol. 86, 1821–1834.

Kołodyńska, D., Wnętrzak, R., Leahy, J.J., Hayes, M.H.B., Kwapiński, W., Hubicki, Z., 2012. Kinetic and adsorptive characterization of biochar in metal ions removal. Chem. Eng. J. 197, 295–305.

Kończyk, J., Kluziak, K., Kołodyńska, D., 2022. Adsorption of vanadium (V) ions from the aqueous solutions on different biomass-derived biochars. J. Environ. Manag. 313, 114958.

Koppula, S., Jagasia, P., Panchangam, M.K., Surya, S.B.M., 2022. Synthesis of bimetallic Metal-Organic Frameworks composite for the removal of Copper (II), Chromium (VI), and Uranium (VI) from the aqueous solution using fixed-bed column adsorption. J. Solid State Chem. 312, 123168.

Laird, D.A., Fleming, P., Davis, D.D., Horton, R., Wang, B., Karlen, D.L., 2010. Impact of biochar amendments on the quality of a typical Midwestern agricultural soil. Geoderma 158, 443–449.

Largitte, L., Pasquier, R., 2016. A review of the kinetics adsorption models and their application to the adsorption of lead by an activated carbon. Chem. Eng. Res. Des. 109, 495–504.

Lee, J., Kim, K.-H., Kwon, E.E., 2017. Biochar as a catalyst. Renew. Sustain. Energy Rev. 77, 70–79.

Li, J., Tian, Y., Zong, P., Qiao, Y., Qin, S., 2020. Thermal cracking behavior, products distribution and char/steam gasification kinetics of seawater Spirulina by TG-FTIR and Py-GC/MS. Renew. Energy 145, 1761–1771.

Li, M., Liu, Q., Guo, L., Zhang, Y., Lou, Z., Wang, Y., Qian, G., 2013. Cu(II) removal from aqueous solution by Spartina alterniflora derived biochar. Bioresour. Technol. 141, 83–88.

Liu, Y., Wang, H., Cui, Y., Chen, N., 2023. Removal of copper ions from wastewater: a review. Int. J. Environ. Res. Publ. Health 20, 3885.

Liu, Z., Xu, Z., Xu, L., Buyong, F., Chay, T.C., Li, Z., Cai, Y., Hu, B., Zhu, Y., Wang, X., 2022. Modified biochar: synthesis and mechanism for removal of environmental heavy metals. Carbon Research 1, 8.

Lopez-Tenllado, F.J., Motta, I.L., Hill, J.M., 2021. Modification of biochar with high-energy ball milling: development of porosity and surface acid functional groups. Bioresour. Technol. Rep. 15, 100704.

Messori, L., Casini, A., Gabbiani, C., Sorace, L., Muniz-Miranda, M., Zatta, P., 2007. Unravelling the chemical nature of copper cuprizone. Dalton Trans. 2112–2114.
Mishra, S., Tiwary, D., Ohri, A., Agnihotri, A.K., 2019. Impact of municipal solid waste landfill leachate on groundwater quality in varanasi, India. Groundwater for Sustainable Development 9, 100230.
Moran, S., 2018. An Applied Guide to Water and Effluent Treatment Plant Design.
Nabuurs, G.-J., Mrabet, R., Abu Hatab, A., Bustamante, M., Clark, H., Havlík, P., House, J., Mbow, C., Kninan, K.N., Popp, A., Roe, S., Sohngen, B., Towprayoon, S., 2023. Agriculture, forestry and other land uses (AFOLU). In: Intergovernmental Panel on Climate, C. (Ed.), Climate Change 2022 - Mitigation of Climate Change. Cambridge University Press, Cambridge, pp. 747–860.
OECD, 2019. Global Material Resources Outlook to 2060 Economic Drivers and Environmental Consequences. OECD publishing.
Ortega, P., Sanchez, E., Gil, E., Matamoros, V., 2022. Use of cover crops in vineyards to prevent groundwater pollution by copper and organic fungicides. Soil column studies. Chemosphere 303, 134975.
Pellera, F.-M., Giannis, A., Kalderis, D., Anastasiadou, K., Stegmann, R., Wang, J.-Y., Gidarakos, E., 2012. Adsorption of Cu(II) ions from aqueous solutions on biochars prepared from agricultural by-products. J. Environ. Manag. 96, 35–42.
Priyanka, Vashisht, D., Ibhadon, A.O., Mehta, S.K., Taylor, M.J., 2024. Enhanced wastewater remediation using mesoporous activated wheat straw biochars: a dye removal perspective. ACS Sustainable Resource Management 1, 355–367.
Priyanka, Vashisht, D., Taylor, M.J., Mehta, S.K., 2023. Evaluating the pre-treatment protocol required to produce an effective carbonized waste adsorbent for organic pollution control. Front. Environ. Sci. 11.
Regmi, P., Garcia Moscoso, J.L., Kumar, S., Cao, X., Mao, J., Schafran, G., 2012. Removal of copper and cadmium from aqueous solution using switchgrass biochar produced via hydrothermal carbonization process. J. Environ. Manag. 109, 61–69.
Renforth, P., Bellamy, R., Beerling, D., Boettcher, M., Bonalumi, D., Brandão, M., Fridahl, M., Fuss, S., Hansson, A., Heyward, C., 2023. Specialty Grand Challenge: Renaming Our Section to "Carbon Dioxide Removal. Frontiers Media SA, 1279109.
Rodriguez, J.A., Lustosa Filho, J.F., Melo, L.C.A., de Assis, I.R., de Oliveira, T.S., 2020. Influence of pyrolysis temperature and feedstock on the properties of biochars produced from agricultural and industrial wastes. J. Anal. Appl. Pyrol. 149, 104839.
Ruz, P., Banerjee, S., Pandey, M., Sudarsan, V., Sastry, P.U., Kshirsagar, R.J., 2016. Structural evolution of turbostratic carbon: implications in H2 storage. Solid State Sci. 62, 105–111.
Shaheen, S.M., Niazi, N.K., Hassan, N.E.E., Bibi, I., Wang, H., Tsang, Daniel C.W., Ok, Y. S., Bolan, N., Rinklebe, J., 2019. Wood-based biochar for the removal of potentially toxic elements in water and wastewater: a critical review. Int. Mater. Rev. 64, 216–247.
Shrestha, R., Ban, S., Devkota, S., Sharma, S., Joshi, R., Tiwari, A.P., Kim, H.Y., Joshi, M. K., 2021. Technological trends in heavy metals removal from industrial wastewater: a review. J. Environ. Chem. Eng. 9, 105688.
Tan, Z., Yuan, S., Hong, M., Zhang, L., Huang, Q., 2020. Mechanism of negative surface charge formation on biochar and its effect on the fixation of soil Cd. J. Hazard Mater. 384, 121370.
Taylor, M.J., Alabdrabalameer, H.A., Michopoulos, A.K., Volpe, R., Skoulou, V., 2020. Augmented leaching pretreatments for forest wood waste and their effect on ash composition and the lignocellulosic network. ACS Sustain. Chem. Eng. 8, 5674–5682.
Tong, X.-j., Li, J.-y., Yuan, J.-h., Xu, R.-k., 2011. Adsorption of Cu(II) by biochars generated from three crop straws. Chem. Eng. J. 172, 828–834.
Tong, X., Xu, R., 2013. Removal of Cu(II) from acidic electroplating effluent by biochars generated from crop straws. J. Environ. Sci. (China) 25, 652–658.
Trakal, L., Šigut, R., Šillerová, H., Faturíková, D., Komárek, M., 2014. Copper removal from aqueous solution using biochar: effect of chemical activation. Arab. J. Chem. 7, 43–52.
Wamucii, S., 2024. United Kingdom (UK) Sugarcane Prices.
Wang, L., Bolan, N.S., Tsang, D.C.W., Hou, D., 2020. Green immobilization of toxic metals using alkaline enhanced rice husk biochar: effects of pyrolysis temperature and KOH concentration. Sci. Total Environ. 720, 137584.
Wijeyawardana, P., Nanayakkara, N., Gunasekara, C., Karunarathna, A., Law, D., Pramanik, B.K., 2022. Removal of Cu, Pb and Zn from stormwater using an industrially manufactured sawdust and paddy husk derived biochar. Environmental Technology & Innovation 28, 102640.
Wu, F.-C., Tseng, R.-L., Juang, R.-S., 2009. Characteristics of Elovich equation used for the analysis of adsorption kinetics in dye-chitosan systems. Chem. Eng. J. 150, 366–373.
Xu, X., Cao, X., Zhao, L., Wang, H., Yu, H., Gao, B., 2013. Removal of Cu, Zn, and Cd from aqueous solutions by the dairy manure-derived biochar. Environ. Sci. Pollut. Control Ser. 20, 358–368.
Xu, Z., Lin, Y., Lin, Y., Yang, D., Zheng, H., 2021. Adsorption behaviors of paper mill sludge biochar to remove Cu, Zn and as in wastewater. Environmental Technology & Innovation 23, 101616.
Xue, Q., Xie, S., Zhang, T., 2022. Chapter 15 - biochar production and modification for environmental improvement. In: Tsang, D.C.W., Ok, Y.S. (Eds.), Biochar in Agriculture for Achieving Sustainable Development Goals. Academic Press, pp. 181–191.
Yang, W., Wang, Z., Song, S., Han, J., Chen, H., Wang, X., Sun, R., Cheng, J., 2019. Adsorption of copper(II) and lead(II) from seawater using hydrothermal biochar derived from Enteromorpha. Mar. Pollut. Bull. 149, 110586.
Zhang, B., Xiong, S., Xiao, B., Yu, D., Jia, X., 2011. Mechanism of wet sewage sludge pyrolysis in a tubular furnace. Int. J. Hydrogen Energy 36, 355–363.
Zhang, C., Zhao, X., Sacchi, R., You, F., 2023. Trade-off between critical metal requirement and transportation decarbonization in automotive electrification. Nat. Commun. 14 (1), 1616. https://doi.org/10.1038/s41467-023-37373-4.